Conducting polymer-ECM scaffolds for human neuronal cell differentiation

ADVANCED HEALTHCARE MATERIALS
www.advhealthmat.de

Conducting Polymer-ECM Scaffolds for Human Neuronal Cell Differentiation

Chiara Barberio, Janire Saez, Aimee Withers, Malavika Nair, Francesco Tamagnini,* and Roisin M. Owens**

3D cell culture formats more closely resemble tissue architecture complexity than 2D systems, which are lacking most of the cell–cell and cell–microenvironment interactions of the in vivo milieu. Scaffold-based systems integrating natural biomaterials are extensively employed in tissue engineering to improve cell survival and outgrowth, by providing the chemical and physical cues of the natural extracellular matrix (ECM). Using the freeze–drying technique, porous 3D composite scaffolds consisting of poly(3,4-ethylene-dioxythiophene) doped with polystyrene sulfonate (PEDOT:PSS), containing ECM components (i.e., collagen, hyaluronic acid, and laminin) are engineered for hosting neuronal cells. The resulting scaffolds exhibit a highly porous microstructure and good conductivity, determined by scanning electron microscopy and electrochemical impedance spectroscopy, respectively. These supports boast excellent mechanical stability and water uptake capacity, making them ideal candidates for cell infiltration. SH-SY5Y human neuroblastoma cells show enhanced cell survival and proliferation in the presence of ECM compared to PEDOT:PSS alone. Whole-cell patch-clamp recordings acquired from differentiated SHSY5Y cells in the scaffolds demonstrate that ECM constituents promote neuronal differentiation in situ. These findings reinforce the usability of 3D conducting supports as engineered highly biomimetic and functional in vitro tissue-like platforms for drug or disease modeling.

1. Introduction

Conducting polymers (CPs) are attractive materials now extensively used in tissue engineering (TE) for cell-based applications.[1–3] CPs display numerous excellent features, such as easy processability, optical transparency, amenability to surface functionalization and chemical modification, high bio- and cyto-compatibility.[4] These properties can be exploited to develop substrates for both small- and large-scale cell cultures by providing a non-invasive way to control cell growth and behavior, as previously described by Langer et al.[5] These polymers enable integration with complex cell cultures in customized 2D or 3D like supports[6–8] and are seen as very promising substrates for neuronal cell growth and differentiation due to their shared electrical and ionic conductivity properties.[9–11] It has been shown that CPs interfacing with living neurons not only enhance neuronal differentiation and growth,[12–15] but are also capable directly interfacing with neurons via the transport of electrons and ions, making them ideal

C. Barberio, A. Withers, R. M. Owens
Bioelectronic Systems and Technology group
Department of Chemical Engineering and Biotechnology
Philippa Fawcett Drive, Cambridge CB3 0AS, UK
E-mail: rmo37@cam.ac.uk

J. Saez
Microfluidics Cluster UPV/EHU
BIOMICs Microfluidics Group
Lascaray Research Center
University of the Basque Country UPV/EHU
Vitoria-Gasteiz 01006, Spain
E-mail: janire.saez@ehu.eus

J. Saez
Ikerbasque
Basque Foundation for Science
Bilbao E-48011, Spain

M. Nair
Cambridge Centre for Medical Materials
Department of Materials Science and Metallurgy
University of Cambridge
27 Charles Babbage Road, Cambridge CB3 0FS, UK

F. Tamagnini
University of Reading
School of Pharmacy
Hopkins Building, Reading RG6 6LA, UK
E-mail: f.tamagnini@reading.ac.uk

The ORCID identification number(s) for the author(s) of this article can be found under https://doi.org/10.1002/adhm.202200941

DOI: 10.1002/adhm.202200941

candidates for engineering neural scaffolds. In contrast to planar electrodes, the CP-based scaffolds provide the ability to create 3D substrates of different form factors with low stiffness and impedance, thus mimicking soft brain tissue.[16–19]

Poly(3,4-ethylenedioxythiophene) polystyrene sulfonate (PEDOT:PSS) is a widely studied CP, with high electrical and ionic conductivity[20] and chemical stability,[21] and has been employed for numerous in vivo and in vitro applications.[22] We recently engineered 3D macroporous electroactive scaffolds, based on PEDOT:PSS for in vitro TE studies[23,24] and organ-on-chip platforms that performed as excellent substrates for hosting 3D cultures of cells undergoing in situ differentiation.[25]

Despite their remarkable performance as tissue engineering substrates for 3D cell culture, CP scaffolds are often more rigid than biological tissues with some propensity to be brittle[6] and display sub-optimal mechanical robustness and stability.[7] Most importantly, the lack of biochemical cues in the context of human tissue equivalents represents a major limitation. These drawbacks could represent a critical hurdle in bioengineering and tissue regeneration, luckily, coating or blending with natural materials (e.g., extracellular matrix or ECM, constituents) represent promising strategies to regulate and improve cell behavior (e.g., adhesion, survival, and proliferation) by providing the microenvironmental cues for a highly favorable niche for cells to grow. Several tissue engineering studies have generated 3D polymer-biomaterial supports to host neuronal cultures in biomimetic conditions.[26–29] However, being able to more closely mimic neural networks in vitro remains very challenging given the physiological complexity of the brain milieu. Also, since neurons are electrically excitable cells, the use of electroactive biomaterials able to support neural growth and effective electrical communications between neurons, is compelling.[30–32]

In the human body, the ECM is a high-water content 3D structure consisting of proteins and polysaccharides which offer tissue support, playing key roles in both cell–cell and cell–ECM interactions. The ECM mediates the diffusion of soluble factors and regulates several cellular behaviors, such as cell adhesion, growth and differentiation.[33,34] Collagen, hyaluronic acid (HA), laminin and other ECM components are attractive biopolymers for in vitro applications, thanks to the possibility to control and tailor their physical and chemical properties for mimicry of the in vivo milieu.[35] Collagen is the most abundant protein in mammalian ECM and normally provides tensile strength, stability and structure, whereas HA is a non-sulfated glycosaminoglycan (GAG) capable of retaining high amount of water, thus maintaining tissue hydration.[36] Laminins are large heterotrimeric components of the basal lamina playing a crucial role in cell adhesion, survival, and differentiation.[37] These structural and functional matrix constituents are highly represented in human tissues, exhibit advantageous properties (e.g., low immunogenicity, biocompatibility, biodegradability, and hydrophilicity),[38] and are therefore ideal candidates as bioactive substrates in TE (e.g., scaffolds, gels, fibers, and sponges).[39–41]

Conducting polymer-based platforms can be fabricated via several techniques, (e.g., electrochemical polymerization, vapor phase deposition)[42] and, as in this study, the freeze-drying (or ice-templating) approach represents an alternative method to engineer free-standing porous 3D scaffolds that enables the inclusion of additives into the dispersions prior to the lyophilization step.[43] Such a strategy is extensively harnessed in bioengineering research to improve the scaffold mechanical stability, biomimicry, and biocompatibility features. Previously, we made PEDOT:PSS-Collagen type I composites and showed in situ differentiation of human neural crest-derived stem cells into osteoblasts. This resulted in a decrease in Young's modulus without compromising electrical conductivity.[25] However, collagen alone is insufficient to mimic the brain ECM.[44,45]

The integration of biomaterial systems to recapitulate the brain ECM configuration for in vitro neuropatho-physiology studies has gained significant interest[29,46–48] given the heterogeneous network of HA, other GAGs, and proteins characterizing the neuronal microenvironment. By acting as tissue-specific biological cues within a 3D format, such biomaterials strategies would allow elucidation of cell–cell and cell–ECM interactions, thus resembling the natural brain tissue milieu more closely. The phenotype, gene expression, and electrophysiology properties of neuronal cells are highly influenced by their immediate extracellular microenvironment; thus, in vitro neuronal cell models benefit from these 3D cell culture formats, as cells are more prone to express the neuronal features and generate more realistic and electrophysiologically active neuronal networks.[49] As previously investigated, the electrophysiological, molecular and morphological properties of neuronal progenitor cells grown in 3D are more similar to the ones of a mature neuron, in comparison to cells grown in 2D formats.[50,51] This may be explained by the fact that a 3D substrate more closely resembles the native environment of a neuron.

Herein, we fabricated 3D PEDOT:PSS porous composite scaffolds integrating collagen, HA and laminin, to support and enhance neuronal cell culture in 3D. We characterized and compared the mechanical, electrochemical, and structural properties of these ECM composites with respect to pristine (PEDOT:PSS only) scaffolds. SH-SY5Y human neuroblastoma cells were seeded and cultured in the scaffolds to evaluate differential biological responses to these substrates. The differentiation of SH-SY5Y cells into mature neurons on the scaffolds was evaluated for capability in promoting neuronal network formation. Finally, the voltage-dependent Na^+ and K^+ currents, input resistance and other electrophysiological features of the SH-SY5Y cells differentiated in the 3D environment were examined. This allowed us to investigate the effect of PEDOT:PSS/ECM composite scaffolds on the maturation of the electrical membrane properties of neurons, establishing our ability to generate functional neuronal networks in 3D, enhanced in the composite CP/ECM scaffolds, compared to the pristine.

2. Results and Discussion

2.1. Fabrication, and Mechanical and Electrochemical Characterization of Composite Scaffolds

We designed and fabricated biocompatible electroactive composite scaffolds tailored for 3D neuronal cell culture. These biomimetic substrates were prepared by blending PEDOT:PSS with increasing concentrations of type I collagen (e.g., collagen low or COL1, collagen high or COL2), a fixed amount of HA and human laminin following the protocol described in Materials & Methods. The rationale of choosing these three molecules

stems from the roles they play in the tissue as major components of the ECM in vivo,[25,19,29,52] thus, their inclusion would render the supports under investigation highly biomimetic. Specifically, we developed one set of PEDOT:PSS porous scaffolds containing only collagen at different concentrations (i.e., COL1, low collagen, 1.5 mg mL^{-1} and COL2, high collagen, 2 mg mL^{-1}—blue arrow in **Figure 1**A. The concentration of collagen used in our composite scaffolds was based on previous literature using collagen as a composite in 3D substrates.[53–55] The scaffolds with collagen only were compared to a second set of collagen-containing scaffolds also including fixed concentration of HA and laminin as additional dispersion constituents (i.e., COL1/HA/LAM, COL2/HA/LAM, green square in Figure 1A). The goal of such approach was two-fold: First, to analyze the effects of the inclusion of these ECM constituents on the scaffold properties and second, to gain a better understanding of their role on cell viability and behavior within the 3D cell-laden generated substrates. All five blends were dispersed into molds and scaffolds were generated via the freeze-drying method and compared to the pristine scaffolds. They set of scaffolds under study are the following: PEDOT:PSS, COL1, COL2, COL1/HA/LAM and COL2/HA/LAM. Similarly to the procedure previously used by Iandolo et al.,[25] the mixtures were dispersed overnight with magnetic stirring at room temperature to avoid dispersion precipitation and achieve homogeneous solutions. The resulting scaffolds were used for seeding, maintaining, and differentiating SH-SY5Y human neuroblastoma cells into mature neurons. Finally, whole-cell patch-clamp recordings were acquired from differentiated SH-SY5Y cells undergone neuronal maturation within the scaffolds to characterize and compare their electrophysiology properties (e.g., voltage-gated Na^+ and I^+ currents). Schematics for the whole strategy are shown below (Figure 1A).

Prior to cell seeding PEDOT:PSS/ECM scaffolds were subjected to mechanical and electrochemical characterization (Figure 1B–E). High-water retention capacity is a key factor which allows cells to adhere and grow within an environment resembling the natural ECM in the body. The swelling index of PEDOT:PSS/ECM composite scaffolds showed a steadily increasing trend of liquid uptake in all samples compared to the control, as displayed in Figure 1B. After 2 h incubation in PBS, COL1 and COL2 had similar liquid uptake capacity to PEDOT:PSS, while the two COL/HA based scaffolds exhibited higher values. (Table S1, Supporting Information). A statistically significant difference in swelling ratio with respect to pristine scaffolds was observed in COL2/HA/LAM ($*p < 0.05$, PEDOT:PSS vs COL2/HA/LAM: 1954%–2983%). Similarly to previous tissue engineering studies using blends of synthetic and natural polymers for scaffolds fabrication,[56–59] we hypothesized that these differences could be attributed to the synergy between the increasing collagen content in all the samples and the presence of HA in the second group, both responsible for promoting more pronounced water retention since they are hydrophilic macromolecules.

Young's modulus is a parameter used to characterize the mechanical properties of elastic materials, such as hydrogels and scaffolds. Generally, in the TE field it is fundamental to define the stiffness and tensile strength of a given biocompatible substrate, since they can be used as a tool to manipulate and control cell phenotypes and thus modulate cell behavior.[35] Moreover, the mechanical features of the scaffold should aim to recapitulate those of body tissues. Young's moduli of each dry scaffold were estimated via compression experiments and the values obtained were calculated from the tangent of the loading curves as reported in Figure 1C and Table S1, Supporting Information. Overall, the reduced stiffness of composite scaffolds was consistent with the remarkable increase in the swelling ratio mentioned above. Specifically, a stepwise decrease in stiffness (kPa) was apparent for all the composite scaffolds in comparison to PEDOT:PSS with 38.1 ± 6.1 kPa as the highest value ($****p < 0.0001$). According to previous studies,[25,56] it is assumed that blending natural additives (i.e., collagen and HA) into PEDOT:PSS solution could reduce the modulus of the latter and therefore render the derived scaffolds more suitable for soft tissue engineering applications. Moreover, increasing the concentration of collagen along with the presence of HA contributed to lowering the stiffness of the composite ECM substrates and thus widened the gap in mechanical robustness between this set of scaffolds and the control. The compressive modulus of native neuronal tissue ranges between 0.1–20 kPa,[31,60-62] given the high content of proteoglycans binding water molecules in the brain parenchyma.[63] Although our composite scaffolds exhibit stiffer mechanical features than the brain tissue, the inclusion of ECM elements still allows a fairly accurate recapitulation in vitro of the chemical and structural properties of the brain ECM and hence have higher potential in biomimicry than those engineered from mere synthetic biomaterials.

To benefit from the electrically conducting properties of the CP which may influence neuronal differentiation, it is important to establish that the inclusion of ECM components does not adversely affect the conductivity of the CP. Electrochemical impedance spectroscopy (EIS) is a sensitive technique extensively used for characterizing electrochemical properties of materials and devices. We employed this method to analyze the effects of incorporating collagen, hyaluronic acid and laminin to the electrochemical properties of PEDOT:PSS. For the EIS measurements, gold was coated on kapton and added to the dispersions prior to the freeze-drying process to obtain scaffold-based electrodes (Figure S1, Supporting Information). As shown in Figure 1D,E, very small differences were found in impedance values for the composite scaffolds compared to the control, pristine scaffolds, meaning that the electrical features were overall maintained. Moreover, despite the addition of ECM components to the pristine polymer solution, all samples were characterized by a flat curve at mid-high frequencies (100–10 000 Hz), as expected in conducting materials.[8] Specifically, COL1 and COL2 composite scaffolds without HA/LAM show slightly higher impedance values in the mid-low frequency range with respect to the pristine PEDOT:PSS scaffolds (Bode plot, Figure 1D) (Nyquist plot, 1D, inset image). This is in line with previous results.[25]

Interestingly, upon integration of HA and laminin in the second set of the COL1/HA/LAM and COL2/HA/LAM, a decrease in impedance was observed within the same frequency range (i.e., 10^3–10^5 Hz:COL1/HA/LAM = 28.7%, COL2/HA/LAM = 30.5%, Figure 1D). These scaffolds displayed slightly higher conductivity in comparison to pristine PEDOT:PSS. This phenomenon could be related to interactions between the collagen and HA/LAM which may enhance the ionic and electronic conductivity of the scaffolds.[64] HA can act as an additional counterion to PEDOT,[65] enhancing its conductivity in the high frequency range (>10^3 Hz).[66] As a negatively charged polysaccharide,

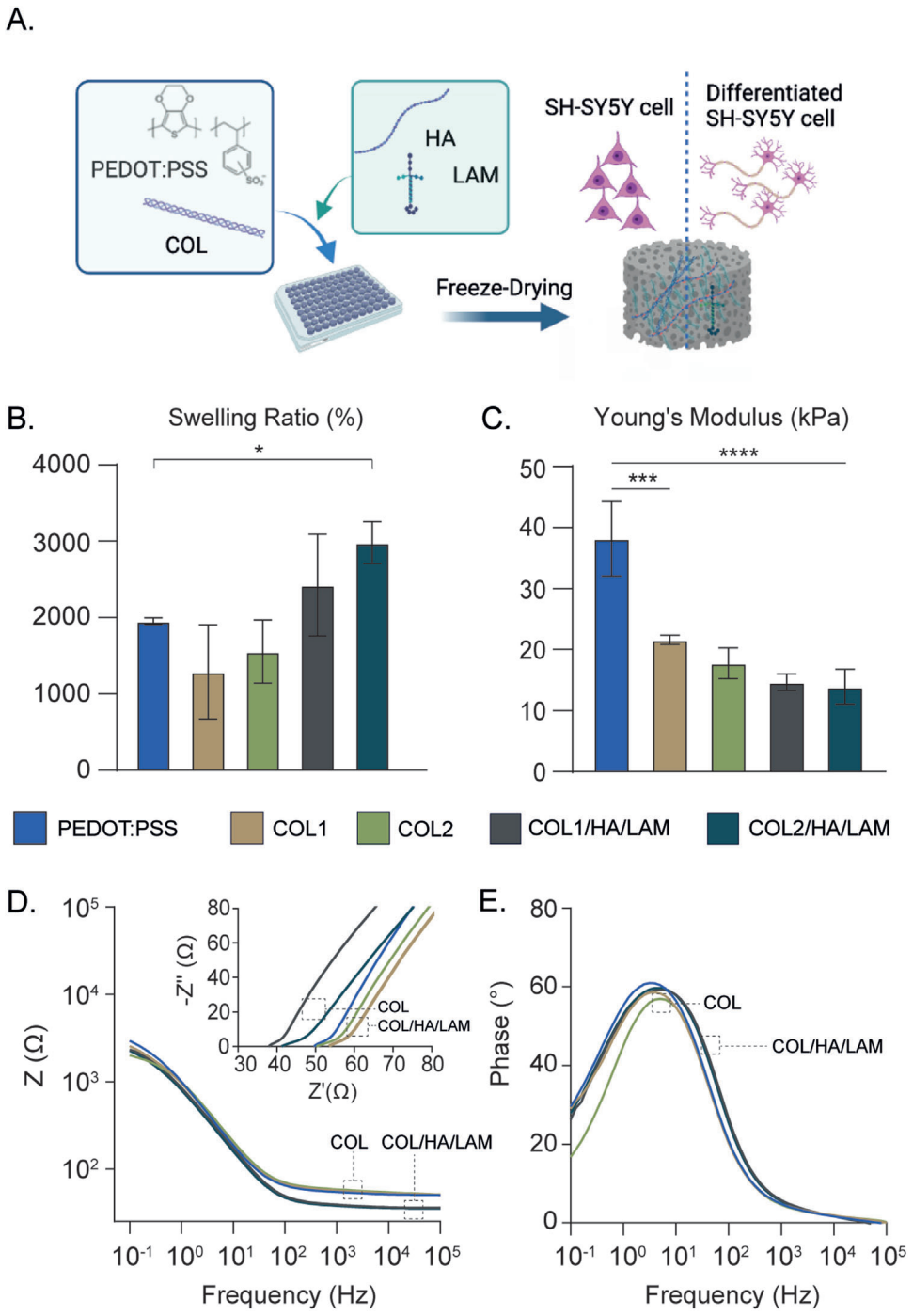

Figure 1. Schematic showing the components and fabrication steps of the 3D PEDOT:PSS/ECM composite scaffolds engineered in this study. A) Left: Blends of PEDOT:PSS, COL1, COL2 (blue arrow) and PEDOT:PSS, COL1/HA/LAM, COL2/HA/LAM (green arrow) were prepared in the 1:1 ratio to form PEDOT:PSS/ECM dispersions at different collagen concentration. Right: The blended scaffolds were used as 3D support for seeding SH-SY5Y human neuroblastoma derived cells and hosting their differentiation into neurons. Created with BioRender.com. B) Bar charts describing swelling ratios (%) and C) Young's modulus of the scaffolds. The difference between pristine and samples was evaluated using one-way ANOVA, with $*p < 0.05$ for swelling capacity and $****p < 0.0001$ for Young's modulus. Error bars represent the standard deviation of three replicates for each condition (mean ± SD, $n = 3$). D) Electrochemical impedance spectroscopy measurements of PEDOT:PSS (blue), COL1(brown), COL2 (light green), COL1/HA/LAM (grey), and COL2/HA/LAM (dark green) composite scaffolds represented by the Bode plot and corresponding Nyquist plot (insets). E) Corresponding phase angle versus frequency graph of the scaffolds showing a slight shift of the phase angle at low frequencies in the COL/HA/LAM set.

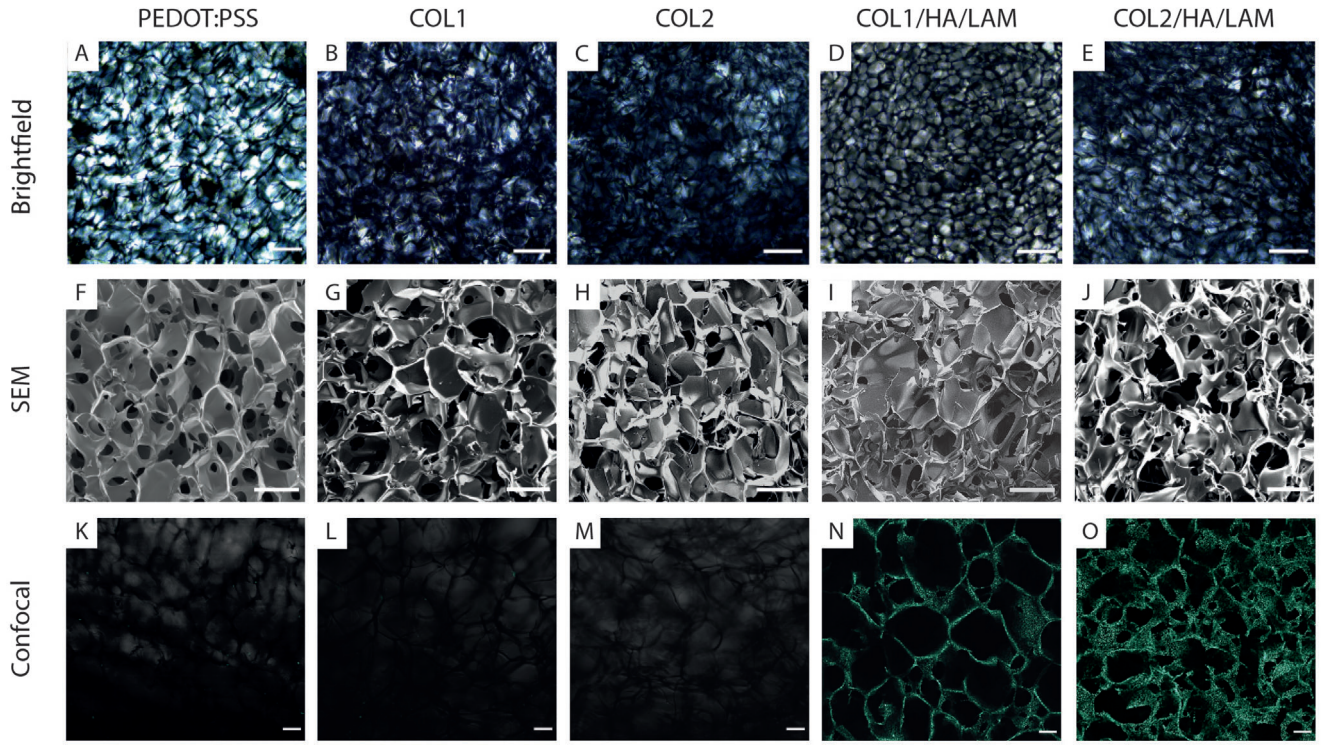

Figure 2. Brightfield, SEM and confocal images of composite scaffolds: PEDOT:PSS (A,F,K), COL1 (B,G,L), COL2 (C,H,M), COL1/HA/LAM (D,I,N), and COL2/HA/LAM (E,J,O). Brightfield: scale bar, 200 μm; SEM: scale bar, 100 μm; fluorescence images: scale bar, 50 μm. The bottom row of confocal microscopy images represents PEDOT:PSS/ECM samples stained for HA using HABP-biotinylated (1:50) and FITC-streptavidin (1:100, green). All the images show the internal microstructure with characteristic highly interconnected porosity.

HA may support ion diffusion normally occurring in the lower frequency range (< 10^2 Hz). These differences are more apparent in the Nyquist plots (Figure 1D, inset) where the curves corresponding to the collagen-only containing scaffold samples are all shifted to higher impedance magnitudes than the pristine (> 50 Ω), whereas HA-collagen-laminin containing scaffolds exhibited lower impedance values (< 50 Ω). Finally, these electrochemical changes between the composites are accompanied by a very slight shift of the phase angle at lower frequencies in the phase angle maximum of COL1/HA/LAM and COL2/HA/LAM scaffolds set with respect to COL1 and COL2 (Figure 1E).

2.2. Scaffold Optical Characterization

Next, we examined the morphology and inner porous microstructure of the composite scaffolds via brightfield microscopy, scanning electron microscopy (SEM) and confocal microscopy (**Figure 2**A–O). All samples exhibit highly interconnected porosity with an average pore size diameter and pore area ranging between 20–25 μm and 470–823 μm^2, respectively (Figure S2, Supporting Information). Furthermore, the brightfield images showed a more ordered and organized pore network in the collagen/HA/LAM-derived scaffolds with respect to pristine and collagen-based samples (Figure 2A–O). By means of SEM, in the PEDOT:PSS/ECM scaffolds it was possible to identify the presence of agglomerates within some areas of the backbone walls (Figure S3, Supporting Information), which were absent both in the control and in the PEDOT:PSS/COL samples. Finally, to optically assess the presence of HA and visualize its spatial organization within the porous backbone of the COL/HA containing scaffolds, a fluorescence staining experiment using a biotinylated hyaluronic acid binding protein (HABP) was performed (Figure 2K–O). Fluorescent signal was detected only in COL1/HA/LAM and COL2/HA/LAM, but as expected, not in PEDOT:PSS (Figure 2K) nor in collagen containing scaffolds (Figure 2L,M). As reported in the set of pictures, HA is evenly dispersed throughout the scaffold backbone (Figure S4, Supporting Information) whose inner porous microstructure is overall well-maintained.

As further step, we tested whether the co-existence of ECM components promotes cell adhesion and proliferation, and whether a highly interconnected pore network of the hybrid scaffolds could provide the optimal microenvironmental cues for improving cell viability, growth, and neuronal differentiation in the long term. Indeed, the existence of highly interconnected pore density in all the hybrid substrates could enhance and maximize such properties by enabling continuous cell media infiltration, nutrients penetration and gas exchange throughout.[67,68]

2.3. 3D Neuronal Cell Culture in Scaffolds

Moving forward to neuronal cell viability experiments using the engineered scaffolds, we investigated whether the integration of physiologically relevant ECM constituents affected or even

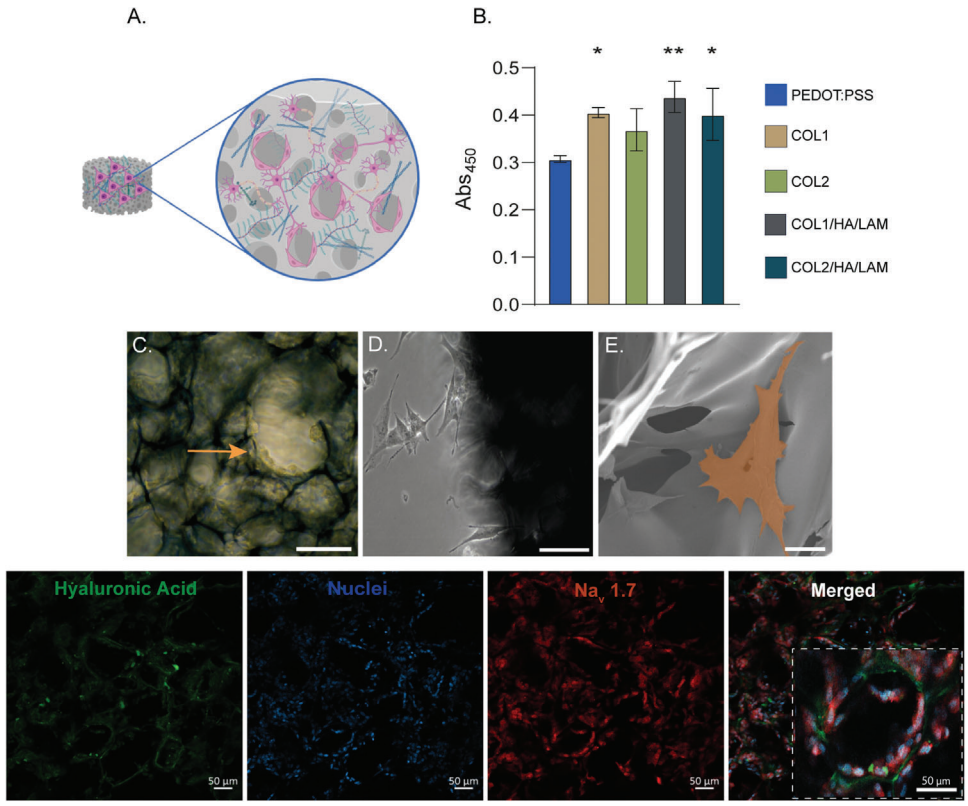

Figure 3. 3D Neuronal cell culture characterization into scaffolds. A) Cartoon of a cell-laden scaffold showing the spatial organization of SH-SY5Y growing in a 3D configuration lining the pores and adhering on the backbone edges. Created with BioRender.com. B) Viability of SH-SY5Y cells measured by XTT assay. Bar chart showing the absorbance at 450 nm of the six samples compared to PEDOT:PSS control. Absorbance values were obtained after 8 days of SH-SY5Y cell culture with initial seeding cell density of 2.3×10^4 cells. Difference between samples and pristine was assessed using one-way ANOVA, $^{**}p < 0.01$. Error bars represent the standard deviation of three replicates(mean ± SD, $n = 3$). C) Brightfield images of COL1/HA/LAM scaffold at day 3 and D) at day 7 after cell seeding. Scale bars 50 and 20 µm, respectively. Orange arrow shows SH-SY5Y cells adhering on one pore wall. E) SEM image of SH-SY5Y cell (false colored orange) adhering on COL2/HA/LAM scaffold walls at day 7 of cell culture. Scale bar 20 µm. F) Composite fluorescence images of immunostained SH-SY5Y cells in COL2/HA/LAM scaffold. The samples were stained for hyaluronic acid (green), nuclei (Hoechst, blue), Na_v 1.7 channel (red), magnification 20×. Scale bar 20 µm. One scaffold pore edged by SH-SY5Y cells is highlighted with white dashed line.

improved the scaffolds cytocompatibility profile for SH-SY5Y human neuroblastoma-derived cells, used herein as neuronal cell line model (Figure 1A).

SH-SY5Y cells have been extensively used, with numerous studies showing that these cells can be differentiated into specific neuronal subtypes.[69,70] We chose to use this cell line as a robust model for screening our scaffolds for their ability to support neuronal growth.

A cell viability assay was carried out aiming to pinpoint any difference in cellular metabolic activities and thus, cell survival of the neuronal cells within the scaffolds. Viability and growth of the cells within the scaffolds was estimated at day 8 of cell culture. For comparison, we also ran the same experiment at higher cell-density (1×10^5 cells) at day 7 of cell culture (Figure S5, Supporting Information). Interestingly, all the blends of PEDOT:PSS/ECM seemed to improve cell survival and proliferation with respect to PEDOT:PSS, regardless of the collagen content (**Figure 3**B and Figure S5, Supporting Information). Taken together, the results obtained from the two cell cultures initiated at different cell seeding densities (i.e., 2.3×10^4 and 1×10^5, respectively), indicated that COL1, COL2/HA/LAM, COL1/HA/LAM provided the optimal combination of environmental cues promoting a remarkable enhancement in cell survival and growth ($^*p < 0.05$, $^{**}p < 0.01$).

We then proceeded to optical characterization of the cell-laden composite scaffolds (COL1/HA/LAM and COL2/HA/LAM). Given the complex molecular composition of the brain ECM,[44] the composite substrates inclusive of collagen, HA and laminin would better resemble the natural brain ECM milieu compared to the collagen-only scaffolds.

SH-SY5Y human neuroblastoma cells were seeded and cultured in situ for 12 days and imaged using brightfield (Figure 3C,D), SEM (Figure 3E and Figure S6, Supporting Information) and confocal fluorescence microscopy (Figure 3F and Figure S7, Supporting Information). We assessed the cell morphology and the 3D spatial cell alignment throughout the scaffold backbone by looking at the expression of a housekeeping neuronal marker, namely Na_v 1.7. As previously postulated, SH-SY5Y cells endogenously express the sodium selective ion channel Na_v1.7 on their membrane.[71]

In both SEM and fluorescence images (Figure 3E,F and Figure S7, Supporting Information), SH-SY5Y cells were found lining the scaffold pore edges instead of proliferating in suspension through its cavities; such an observation supports our initial

hypothesis about the role of PEDOT:PSS as scaffolding support for 3D cell culture. Together with the XTT cell viability results (Figure 3B), the data show that such structural and mechanical role played by the pristine scaffolds are even enhanced and improved in the COL1/HA/LAM and COL2/HA/LAM samples, where the inclusion of ECM elements within the blends increases neuronal cell attachment, growth and thus proliferation capability.

2.4. 3D Neuronal Cell Culture Differentiation in Scaffolds

Although extensively used as in vitro neuronal cell culture model for many applications in the field of neuroscience research, SH-SY5Y cells are human immortalized and undifferentiated cells expressing markers indicative of immature neurons.[70,72,73] Upon differentiation, SH-SY5Y cells exhibit an increased plasma membrane excitability, functional synapses, branched processes, long neurites, and express a variety of different mature neural markers (e.g., MAP, SYN). Therefore, differentiated SH-SY5Y cells can be considered as a reasonable model of mature neurons in the context of translatable 3D in vitro human biomimetic studies. To our knowledge, only a few studies have been conducted on the differentiation of human neuroblastoma cells in 3D electroactive supports, such as conducting polymer scaffolds[10] and carbon nanotubes (CNT).[74] However, the additional inclusion of biomimetic components of the brain ECM to better support neuronal differentiation has never been attempted. Herein, we use PEDOT:PSS substrates integrating ECM components to host and enhance neuronal maturation. We implemented a differentiation strategy based on the addition of RA and BDNF to the culture medium of the hybrid scaffolds engineered in this study[69,75] (**Figure 4**A). The preliminary effects of PEDOT:PSS (control) and COL2/HA/LAM samples on neuronal differentiation and neural marker expression were investigated. The COL2/HA/LAM scaffolds were chosen as displaying optimal swelling capacity and Young's modulus, with the additional benefit of showing the lowest impedance values in the mid-high frequencies range with respect to all other candidates (Figure 1C–H). This property is essential to detect very small changes in real-time electrical monitoring of 3D cell culture growth within scaffolds porous architecture for future applications.[76] The combination of collagen/HA/laminin in the scaffold was also thought to be advantageous in terms of homogeneously supporting SH-SY5Y cell attachment to initiate and undergo subsequent neuronal differentiation. After culture for 12 days in the differentiation medium (see Experimental Section), immunostaining of β-tubulin-III (red) and MAP-2 (orange), two of the most expressed neuron-specific markers upregulated in mature neuronal cells[69,77] was performed in order to visualize differentiated neurons and their neurite extensions within the 3D cell-laden scaffolds. Overall, as shown in Figure 4B–E, both PEDOT:PSS and COL2/HA/LAM scaffolds displayed confluent 3D neuronal networks formed throughout the bulk of the scaffold with intimate cell–cell interaction. Interestingly, most of the neurite outgrowth was seen transversally crossing the pores diameter from side-to-side (Figure 4B–E, zoomed insets; Figure 4H; Figure S8, Supporting Information). We also observed that both cell density and neurite outgrowth in COL2/HA/LAM were increased when compared to the control. When neuronal differentiation occurs, mature neurons are expected to express both MAP-2 and β-tubulin-III in their elongated axons with a lower proliferation rate with respect to the immortalized undifferentiated cells. In support of our hypothesis that ECM elements promote and support neuronal differentiation and neurite extension, confocal images showed that the fluorescence intensity of both MAP-2 and β-tubulin-III is ≈2 times and ≈1.5 times higher, respectively, in differentiated SH-SY5Y cells grown within the hybrid scaffold than in PEDOT:PSS ($^{**}p < 0.01$, Figure 4F and Figures S8 and S9, Supporting Information). Neurite length (μm) of differentiated neurons was estimated using the NeuronJ plugin. As reported in the boxplots in Figure 4G and Figure S10, Supporting Information, differentiated SH-SY5Y cells in COL2/HA/LAM scaffolds exhibited longer axonal length ranging between 20.5–155 μm (MAP-2) and 22.6–137.7 μm (β-tub) with respect to the control (12.1–94.6 μm, MAP-2 and 14.7–101.2 μm, β-tub). Overall, the data corroborate that SH-SY5Y cells undergoing differentiation within ECM-based hybrid scaffold reveal higher propensity to adhere and proliferate onto surface areas where ECM components are more densely expressed (Figure 4H–J) and exposed for binding, following in situ neuronal networks generation.

2.5. Electrophysiology Recordings of Differentiated Cells in Scaffolds

The use of electrophysiology to record the electrical single and network neuronal activity is essential to gain more insight into the functional properties of nerve tissue. Several studies have shown neuronal differentiation from SH-SY5Y neuroblastoma cells in electrically conducting supports[10,74,78,79]; however, the resulting neuronal networks have not been functionally characterized using the gold standard patch-clamp technique. We used whole-cell patch-clamp recordings to both demonstrate neuronal maturation as well as investigate the changes in electrical properties of differentiated SH-SY5Y cells grown in 3D PEDOT:PSS and COL2/HA/LAM scaffolds (**Figure 5**A). Recordings were made from differentiated cells grown for 12 days in composite and pristine scaffolds.

Patch-clamp allows the measurement of different parameters of a neuron, such as membrane input resistance (R_{in}), action potentials (AP) and the biophysical properties of the voltage-gated membrane channels underlying their generation, such as non-inactivating, voltage-gated, K^+ channel maximal conductance (G_{max}) and half-activation voltage ($V_{1/2}$).

We observed that a portion of the cells patched ($n = 8$ in PEDOT:PSS and $n = 10$ in COL2/HA/LAM) developed action potentials as well as the underlying voltage-gated inward, Na^+ mediated and outward, K^+ mediated currents, in each condition (Figure 5B,C). We measured the biophysical properties of the non-inactivating, outward, voltage-gated K^+ current because this current could be consistently observed in all the cells. No difference was observed in the G_{max} and the $V_{1/2}$ of the outward, non-inactivating K^+ conductances between the cells grown in COL2/HA/LAM in comparison to the PEDOT:PSS control condition (Figure 5D–F). This means that the composition of the scaffold does not affect this current, which is common to

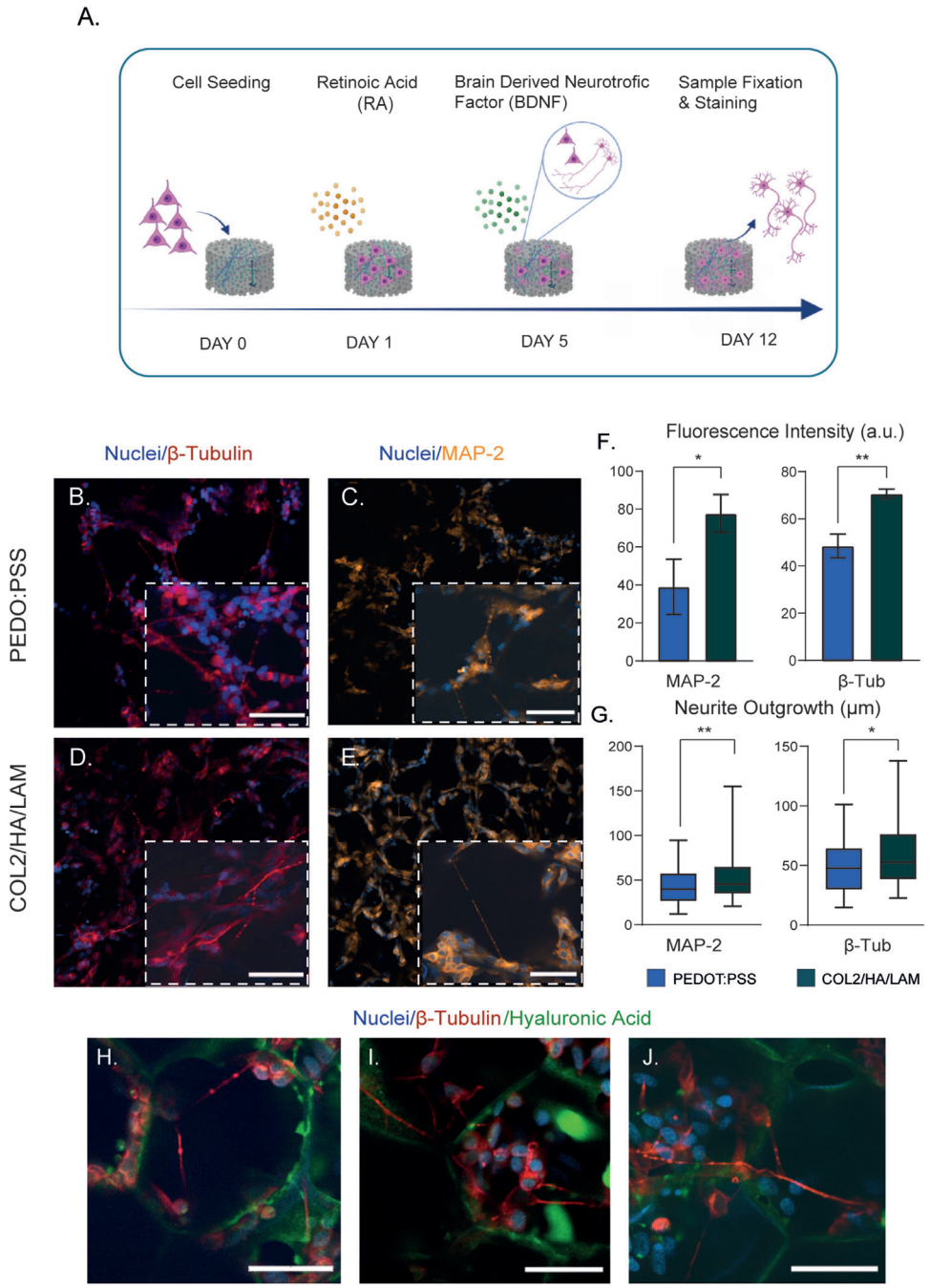

Figure 4. 3D Neuronal differentiation in scaffolds. A–D) Immunostaining of neuronal protein markers in SH-SY5Y cells grown in scaffolds and undergone differentiation after 12 days of treatment with 10 μm RA and 50 ng mL^{-1} BDNF. A) Figure created with BioRender.com. Specifically, PEDOT:PSS (B,C) and COL2/HA/LAM (D,E) were used to maintain and host neuronal differentiation. SH-SY5Y cells were stained both for β-tubulin using eFluor570 (red), MAP-2 using AF555 (orange) and counterstained with Hoechst (blue). Scale bar, 50 μm. Quantification of MAP-2 and β-tub fluorescence intensity (F) and neurite outgrowth (G) in PEDOT:PSS and COL2/HA/LAM samples. Welch's test and unpaired Mann–Whitney U test were used to analyze differences between samples, respectively. In (F), error bars represent the standard deviation of three replicates (mean ± SD, $n = 3$), $*p < 0.05$, $**p < 0.01$. G) In the boxplots, the bar shows the median, and the upper and lower boxes represent the 75% and 25% of the data, respectively. The end of the upper whisker and the end of the lower whisker represent the maximum and minimum value, respectively, of the data set. H–J) Panel of three images with a group of differentiated neurons adhering on clusters of collagen and HA (green) with neurites extending across the pores in COL2/HA/LAM scaffold. Scale bar, 20 μm.

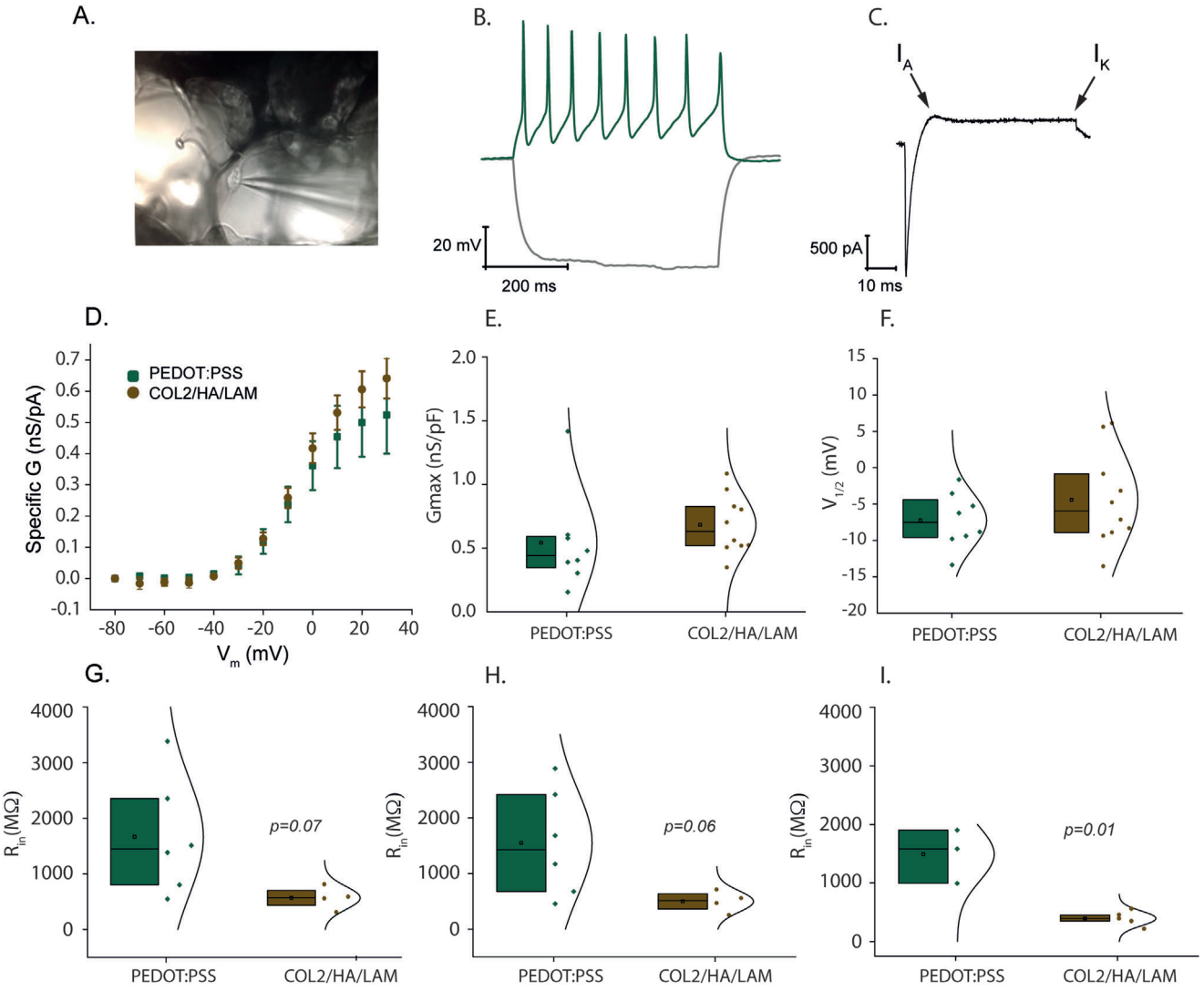

Figure 5. The addition of ECM components to PEDOT:PSS reduces the R_{in} at depolarized potentials in differentiated SH-SY5Y cells. A–C) Neuronally differentiated SH-SY5Y cells were patch-clamped in whole-cell configuration (A); some of them showed action potentials (B) and the underlying voltage-gated inward and outward currents. The outward K^+ current could be differentiated into a fast inactivating (I_A) and non-inactivating (I_K) component (C). D–F) *I–V* curves were built for measuring the biophysical properties of the I_K. Error bars are mean ± SD, $n = 8$ for PEDOT:PSS, and $n = 10$ for COL2/HA/LAM (D). Single Boltzmann fits were used to calculate E) the maximal conductance (G_{max}) and F) the half-activation voltage ($V_{1/2}$) of the channels mediating this current. G–I) The R_{in} of these cells was reduced in COL2/HA/LAM at more depolarized potentials (I) but shy of significance at more hyperpolarized ones (G,H). An unpaired *t*-test was performed to determine the level of significance. Each experiment was carried out with at least three biological replicates (mean ± SD, $n = 3$) where $^*p < 0.05$ was considered statistically significant.

both excitable and non-excitable cells and plays a key role in the generation of action potentials and sustained firing.[80] The effect of the addition of collagen, HA and laminin to PEDOT:PSS on the electrical resistance of the plasma membrane of the cells (R_{in}) was then measured at fixed pre-stimulus potentials of −65, −59, and −51 mV (these values are not corrected for the junction potential). This approach allowed measurement of the R_{in} at different membrane potentials while removing the bias arising from cell-to-cell variability in the resting membrane potential. In addition, we could test the effect of the different scaffolds over R_{in} across three different membrane potentials, as these may have an interaction with the scaffold in generating an effect.[81] We observed that cells grown on composite scaffolds show a general trend for lower R_{in} and smaller intercellular variability (F-test two-sample for variances performed for all pre-stimulus potentials, with $P(F \leq f)$ one tail = 0.01 or 1%). At $V_m = -65$ mV (Figure 5G) and $V_m = -59$ mV (Figure 5H), the R_{in} reduction although not quite statistically significant (unpaired *t*-test; $p = 0.07$ and $p = 0.06$, respectively) shows a trend toward a reduced value. However, at $V_m = -51$ mV, the R_{in} reduction associated with the composite scaffolds is significant (Figure 5I, unpaired *t*-test $p = 0.01$). The R_{in} values recorded for cells grown in the ECM composite scaffolds are closer to those observed in mature differentiated neurons (10–10^2 MΩ), whereas those observed in cells grown on PEDOT:PSS alone are higher and more typical of undifferentiated cells (10^2–10^3 MΩ).[82] Overall, the results

from the patch-clamp experiments indicate that the composite scaffolds contribute to an enhanced, more mature neuronal phenotype compared to the pristine scaffolds.

3. Conclusion

In conclusion, by combining the advantages of conducting polymers and bioactive molecules, 3D electroactive composite PEDOT:PSS/ECM scaffolds were engineered introducing ECM components; collagen type I, HA, and laminin. Although collagen type IV is the most abundant collagen in the brain, collagen type I has been extensively used for neural tissue-engineered equivalents as an excellent substitute and easily available biomaterial which enables remarkable neurite outgrowth in 3D.[83] The mechanical, electrical, and cytocompatibility properties were investigated showing that the composite scaffolds had reduced stiffness and Young's modulus, enhanced conductivity and increased cell proliferation. These composite ECM-derived scaffolds were employed to host and support the differentiation of SH-SY5Y cells into mature neurons. Confocal fluorescence images along with quantitative evaluation of neurite outgrowth corroborated our hypothesis that ECM components present in the COL2/HA/LAM scaffolds promote and enhance neuronal maturation as well as enhanced neurite elongation. Electrophysiology results showed that PEDOT:PSS is a viable scaffold for growing functional neurons differentiated from immortalized human neuroblastoma cells. However, the blending of PEDOT:PSS with ECM constituents was shown to result in a reduction of the membrane R_{in} to values which are associated with more mature neural phenotypes. To our knowledge, this is the first time that such technique is conducted on 3D porous conducting scaffolds to demonstrate neural maturation.

We believe that the electroactive PEDOT:PSS/ECM scaffolds used here to host 3D neural cell culture, could be further employed in tissue engineering as conductive substrates to gain more insights into the physical and biochemical factors influencing cellular behavior in a 3D scaffold configuration and extended to other tissue types (e.g., cell lines, spheroids, organoids).

Future work will focus on leveraging the electrical properties of the CP scaffolds to not only host the neural cultures, but also to monitor them. This is in line with ongoing work in our group engineered customized electroactive porous scaffolds for continuous monitoring of 3D mammalian cell co-cultures.[84,85] Applied to the present study, this will be very relevant for the development of a comprehensive model of the neurovascular unit, which integrates the blood brain barrier (BBB) and the neural (neurons, astrocytes, microglia) components in 3D. Ultimately, such research will be particularly apt for investigating the effects of the microbiome on the brain[86] and for coupling the in vitro bioelectronic humane intestine model recently developed in our group[68] with the neural tri-culture based module.

4. Experimental Section

Scaffold Fabrication: PEDOT:PSS electroactive scaffolds were fabricated using the freeze-drying technique, in which an aqueous dispersion of PEDOT:PSS (Clevious PH 1000, Heraeus Holding GmbH) was mixed with (3-glycidoxypropyl) trimethoxysilane (3 wt%, GOPS, Sigma-Aldrich), a common substrate adhesion enhancer and cross-linker, and (0.5 wt%) dodecylbenzenesulfonic acid (Sigma-Aldrich), a well-known surfactant which improves the conductivity of the film when present in low concentrations.[25,76]

This mother formulation was used to fabricate conducting scaffolds (i.e., pristine) for the 3D neural cell culture presented in this work. Different blends of PEDOT:PSS and collagen type I previously hydrated and homogenized in 0.1 M acetic acid (from Bovine dermal collagen, DEVRO), hyaluronic acid (2 mg mL^{-1}, AbCam), and human laminin, (0.25 mg mL^{-1}, Sigma Aldrich) were formulated. These dispersions were prepared in 1:1 ratios (i.e., 1:1 PEDOT:PSS : COL/HA/LAM) at increasing concentrations of collagen (i.e., 1.5 and 2 mg/mL^{-1}). Afterward, cylindrical wells of a 96-well plate were filled with 150 µL of final solution and then placed in a freeze dryer (VirTis Advantage Freeze Dryer, Wizard 2.0 control system, SP Scientific), to undergo lyophilization from 5 to −35 °C at a controlled cooling rate of −0.22 °C min^{-1} followed by a sublimation phase of 18 h. Subsequent sublimation of ice crystals led to macroporous sponge-like scaffolds. After annealing at ≈45 °C for 4 h to allow crosslinking to occur, the cylindrical scaffolds were cut with the use of a Vibratome (Leica Biosystems) into circular slices of ≈5 mm diameter and 500 µm thickness. In this study, the scaffold slices were employed for preliminary cell seeding experiments, in which they were immersed in ethanol overnight and the following day thoroughly rinsed with sterile water and PBS (Dulbecco's Phosphate Buffered Saline, Sigma Aldrich) under sterile conditions prior to cell seeding.

Optical and Mechanical Characterization of PEDOT:PSS/ECM Composite Scaffolds: The microstructure and surface morphology of the PEDOT:PSS/ECM scaffolds were analyzed using SEM (Leon ZEISS GmBH). First, the samples were removed from the well plate and cut longitudinally and transversely in order to visualize pore orientation from both sections. For bare scaffold visualization, samples were mounted on an aluminum stub with carbon conductive tape. Upon cell seeding, to evaluate cell penetration within the pores, samples were first fixed in 4% paraformaldehyde (PFA) for 12 min at room temperature, washed thoroughly with PBS, dehydrated in a graded ethanol series and then in hexamethyldisilazane solution (Sigma Aldrich) for complete dehydration. The beam voltage used was 1 kV and the number of photons emitted was kept between 5k and 6k on average. Image adjustment and analysis were performed using ImageJ. The compressive moduli of dry scaffolds were performed using a Tinius Olsen 1–50 kN (Tinius Olsen Ltd, UK). The Tinius Olsen had a load cell of 25 N and the compression speed was set at 1 mm min^{-1}. Young's modulus values were calculated from the slope of the linear part of the strain stress curve.

Pore Size Distribution of Scaffolds: The pore size and area analysis of the scaffolds were performed analyzing SEM micrographs as previously described elsewhere.[8,25] For each condition, 25 pores were randomly selected, and their diameter and corresponding area were manually measured using ImageJ. Next, data plotting and statistical analysis were performed using GraphPad Prism9.0.0(121) Software.

Swelling Ratio Analysis: The swelling ratio (SR) analysis was done by immersing the scaffolds in PBS for 2 h at room temperature. The samples were weighed prior to soaking in liquid solution and their dry weight (W_d) was recorded. After immersion, they were gently dried with tissue paper and weighed again for the wet weight (W_w) estimation. According to the well-established equation for the scaffolds swelling (L) calculation,[67] $L = \frac{Ww - Wd}{Wd} \times 100$, different SR values were obtained for each sample. Three slices per scaffold were used for statistical robustness and variability accuracy. Bar charts were obtained and statistically analyzed with GraphPad Prism9.0.0(121).

Electrical Characterization of PEDOT:PSS/ECM Composite Scaffolds: Impedance analysis was performed with a potentiostat (Autolab PGSTAT128N) in a two-electrode configuration. For all the measurements, gold scaffold-based electrodes were fabricated and inserted into the liquid dispersions before undergoing lyophilization. A platinum (Pt) mesh electrode as the counter and reference electrode and the PEDOT:PSS scaffolds were employed as working electrodes with the attachment of a gold-plated Kapton. The AC current was recorded within a frequency range of

0.1–10^5 Hz, with equally spaced data point on a logarithmic scale and 10 data points per decade. The amplitude of the wave sine was 0.01 V_{RMS}. The impedance analysis was performed by creating Bode plots and Nyquist plots derived from different experimental conditions using GraphPad Prism9.0.0(121) Software.

Immunofluorescence and Images: For immunofluorescence staining, cell-laden scaffold slices were fixed with 4% PFA in PBS for 20 min at r.t. Samples were washed three times in PBS and blocked with 1% bovine serum albumin (BSA, Fisher BioReagents) in 0.01% Tween20 for 2 h at room temperature. After washing three times in PBS, samples were incubated with HABP, biotinylated (HABP, 1:100, Sigma-Aldrich), and rabbit primary antibody anti-Nav1.7 (1:150, Alomone Labs, Jerusalem) in 1% PBS-BSA overnight at 4 °C. The following day, scaffold slices were washed three times in PBS and incubated with 1:200 FITC-Streptavidin (ThermoFisher) and 1:200 anti-rabbit secondary antibody Alexa647 (AbCam) in PBS for 2 h at r.t. Finally, after washing thrice with DPBS, cells were incubated for 30 min with DAPI (4',6-diamidino-2-phenylindole, dihydrochloride, Invitrogen) and rinsed three times with PBS. Final samples observation was performed with the confocal microscope (ZEISS LSM 800). For differentiation immunofluorescence staining: Samples were permeabilized in 0.1% Triton X-100 (Sigma-Aldrich) in PBS for 45 min at room temperature, followed by three times washing in PBS. Upon 2 h incubation in 1% BSA-PBS, samples were washed three times in PBS and incubated with rabbit anti-MAP-2 polyclonal primary antibody (1:150, ThermoFisher) in 1% BSA-DPBS buffer and beta-3 Tubulin monoclonal antibody eFluor 660 (5 μg mL^{-1}, ThermoFisher) overnight at 4 °C. On day 2, scaffold slices were washed three times in PBS and incubated with goat anti-rabbit AlexaFluor555 (4 μg mL^{-1}, ThermoFisher) for 2 h RT. After washing thrice with DPBS, slices were incubated with Hoechst (4 μM, AbCam) for 45 min and rinsed again three times before imaging. All images were acquired using a confocal microscope (Axio Observer Z1 LSM 800, Zeiss) with the detector gain value of 650 V for all channels except for one PEDOT_MAP2 picture captured at 620 V to avoid saturation. Images were processed (n = 3 independent images per sample) and analyzed with ImageJ. Fluorescence intensity was quantified after splitting the acquired images in RGB stack channels and then using the red channel of each image for binary masking. The intensity threshold level was kept constant in the range between 20–255 and the fluorescence intensity was obtained and compared for both biomarkers. Neurite outgrowth analysis was performed using the semi-automated ImageJ plugin, NeuronJ, allowing the manual tracking and measurement of all neurites. From each β-tub and MAP-2 fluorescence image, neurites were manually traced and the min, max, mean value, and standard deviation for each measurement were calculated.

SH-SY5Y Cell Culture: Human SH-SY5Y neuroblastoma cells (European Collection of Cell Cultures, ECACC, Sigma-Aldrich) are a cellular sub-line cloned from original SK-N-SH line from neuroblastoma tumor cells, with neuronal-like morphology, some neuronal markers, and the ability to evoke spikes when stimulated by depolarizing steps.[87] SH-SY5Y cells were maintained in 1:1 Minimum Essential Media (MEM; Sigma Aldrich) and Nutrient Mixture F-12 Ham (Sigma-Aldrich) with 15% fetal bovine serum (FBS, Life Technology Invitrogen, US) and 1% non-essential amino acids (NEAA 100X, Sigma Aldrich) and 1% Glutamax 1–100X (Life Technologies). MEM and F12 Medium were complemented with 1% antibiotic-antimytotic 1% penicillin–streptomycin (Sigma Aldrich). Splitting was performed at 70–80% confluency and medium refreshed every other day. In brief, after overnight incubation at 37 °C in 75 cm^2 flasks, cells were washed twice with 6 mL DPBS, then incubated with 4 mL 0.25% Trypsin-EDTA (Invitrogen) for 4 min at 37 °C, 5% CO2, and finally, they were resuspended in 6 mL of fresh culture medium to stop trypsinization. Upon centrifugation at 1000 rpm × 5 min at 20 °C, the medium was aspirated and the pellet was resuspended in fresh culture medium, counted in a hemocytometer, and seeded in new T-75 flasks with a final cell density of 1×10^4 cells cm^{-2}. Prior to seeding on PEDOT:PSS/ECM-based scaffolds, the slices were transferred to a 12-well plate, sterilized for 30 min in ethanol 70%, and then washed three times with DPBS (modified, without calcium chloride and magnesium chloride, sterile, filtered, Sigma Aldrich) and sterile water. Afterward, scaffold slices were incubated in SH-SY5Y growth cell medium for 2 h at 37 °C enabling nutrients and protein absorption within the scaffold. Upon medium removal, cells were seeded onto the slices at two different cell densities (e.g., 23×10^3 and 100×10^3 cells per slice) and incubated for another 2 h at 37 °C. An additional 1 mL of cell medium was added to each well, and the 12-well plate was then incubated at 37 °C, 5% CO_2 for 14 days. Medium was changed every other day.

The differentiation protocol was performed based on previous studies[70,74] modified with some adjustments: Briefly, 1×10^5 SH-SY5Y was seeded on PEDOT:PSS/ECM scaffold slices previously incubated for 2 h in 10%FBS culture media (day 0). On day 2, cell media were replaced with 3%FBS culture media + 10 μM retinoic acid (RA, Sigma-Aldrich) and changed every other day. On day 6, cells were washed once with DPBS and incubated with 3%FBS culture media containing Neurobasal medium (Life Technologies) supplemented with B-27 (ThermoFisher) and 50 ng mL^{-1} brain-derived neurotrophic factor (BDNF, ThermoFisher). Media change occurred every 3 days, and cells were fixed after 12 days of differentiation for preliminary immunofluorescence imaging.

Cell Viability of SH-SY5Y Cells on Scaffolds: Assessment of cell viability and proliferation of SH-SY5Y cells was performed using the XTT Cell Viability Assay Kit (CellSignallingTechnology, Inc., UK) which consisted of an indirect quantitative colorimetric assay detecting the cellular metabolic activities. In brief, SH-SY5Y on scaffold slices were cultured in 24-wellplate for 14 days and used for this assay at day 7 (23×10^3 cells) and day 8 (100×10^3 cells), respectively, to quantitatively monitor cellular growth at the mid-point of the cell culture experiment. After replacing culture media with 400 μL of fresh media, 100 μL yellow tetrazolium salt XTT solution was added to each well. This reagent undergoes reduction into a highly colored formazan dye by dehydrogenase enzymes in metabolically active cells, enabling the estimation of live cells within a given cell culture.

After 3.5 h incubation at 37 °C, 100 μL sample was collected from each well containing scaffold slices and transferred to a 96-wellplate, followed by absorbance reading at 450 nm using a Tecan Spark microplate reader. To extrapolate a quantitative estimation of the cell density for each condition, a sigmoidal standard curve was calibrated for cell number estimation (Figure S5, Supporting Information).

Electrophysiology Recording: Circular, 500 μm thick scaffold slices containing differentiated SH-SY5Y cells at day 14 were transferred to a recording chamber and continuously perfused with HBSS containing 130 mM NaCl, 3 mM KCl, 10 mM HEPES free acid, 2 mM $CaCl_2$, 1 mM $MgCl_2$, and 30 mM D-glucose, and maintained at 34 °C with a temperature control system (Scientifica, UK). Neurons were visualized with an infrared, differential interference contrast microscope (Scientifica, UK). Borosilicate glass micropipettes were pulled with a horizontal puller (Sutter, USA) to an access resistance of 5–9 MΩ. Single micropipettes were filled with intracellular solution containing 145 mM K-gluconate, 5 mM NaCl, 10 mM HEPES, 0.2 mM EGTA, 0.3 mM Na2-GTP, 4 mM Mg-ATP, pH 7.2, 280–290 mOsm per L. Following the obtaining of a stable whole-cell configuration, a junction potential V_j = 15 mV arose due to the difference in composition between intracellular and extracellular solutions. All signals were amplified with a Multiclamp 700B amplifier and digitized using a Digidata 1550B. For whole cell, current-clamp recordings, a hyperpolarizing current step (500 ms, −30 pA) was injected and the consequent plasma membrane voltage (V_m) deflection was measured at the steady state. The ability of a cell to fire action potentials was tested by injecting depolarizing current steps of amplitudes comprised between 10 and 300 pA. The input resistance was calculated based on the Ohm's law: $R = V\ I^{-1}$. To avoid the possibility of bias arising from cell-to-cell variability of the resting membrane potential, all recordings were conducted in the presence of a constant current, holding the pre-stimulus potential at V_m = −65, −59, and −51 mV, respectively (values non-corrected for junction potential). The junction potential could be arithmetically subtracted to each recording, but it did not affect the measurable outcome. However, fixing the pre-stimulus potential at a given value had the double benefit of: i) avoiding the biasing effects of cell-to-cell variability in resting membrane potential over the input resistance; ii) measuring the effect of a given independent variable (i.e., scaffold composition) over a dependent variable (i.e., R_{in}) at different membrane potentials. This was important because at different potentials there might be different voltage-gated conductances open. In fact, a difference between scaffolds was observed on the R_{in} at

depolarized but not as much at hyperpolarized potentials. There was almost a perfect linear relationship between V_m and *p*-values. The voltage-clamp recordings of current–voltage (*I–V*) curves for measuring the properties of voltage-gated, non-inactivating, outward currents were carried out as follows. The series resistance was compensated for (10%–95% correction) and the capacitance of the pipette neutralized. Outward, non-inactivating, voltage-gated currents were evoked by applying $n = 12$, 30 ms, 10 mV voltage steps, starting from an initial holding voltage $V_h = -90$ mV. Each recorded current was leak subtracted and normalized to membrane capacitance to measure the specific current and avoid biases due to cell-to-cell variability in size. The specific conductance (G) was calculated as the ratio between the specific current and the electrochemical force for potassium ($E_K = 100$ mV). Cell-to-cell Boltzmann sigmoidal fit was used to estimate the maximal specific conductance (G_{max}) and the half-activation voltage ($V_{1/2}$) for each neuron.

Statistical Analysis: Analysis of statistical differences was performed, specifically: One-way ANOVA analysis was used for scaffolds mechanical property comparison and for XTT cell viability assay. Welch's test and Mann–Whitney U test were employed for estimating differences in fluorescence intensity and neurite outgrowth, respectively. Unpaired *t*-test was used for analyzing all the membrane properties as described in the Electrophysiology section. Statistical analysis was performed with GraphPad Prism9.0.0(121). Data were represented as mean ± standard deviation.

Supporting Information

Supporting Information is available from the Wiley Online Library or from the author.

Acknowledgements

The authors wish to acknowledge funding from the European Research Council (ERC) under the European Union's Horizon 2020 research and innovation programme (grant agreement no. 723951) (R.O. and C.B.). The authors also wish to acknowledge funding by the Engineering and Physical Sciences Research Council Centre for Doctoral Training in Sensor Technologies and Applications (EP/L015889/1 to C.B.). This project has also received funding from the European Union's Horizon 2020 research and innovation programme under the Marie Skłodowska-Curie (grant agreement No. 842356). The authors would also like to thank Chrysanthi-Maria Moysidou for her precious help with the acquisition and editing of confocal fluorescence images.

Conflict of Interest

The authors declare no conflict of interest.

Data Availability Statement

The data that support the findings of this study are available from the corresponding author upon reasonable request.

Keywords

3D biology, electrophysiology, extracellular matrix, in vitro cell culture, neuronal differentiation, scaffolds

Received: April 25, 2022
Revised: July 23, 2022
Published online:

[1] L. H. Jimison, J. Rivnay, R. M. Owens, *Organic Electronics: Emerging Concepts and Technologies*, Wiley, **2013**, p. 27.
[2] B. Guo, P. X. Ma, *Biomacromolecules* **2018**, *19*, 1764.
[3] R. Balint, N. J. Cassidy, S. H. Cartmell, *Acta Biomater.* **2014**, *10*, 2341.
[4] X. Strakosas, B. Wei, D. C. Martin, R. M. Owens, *J. Mater. Chem. B* **2016**, *4*, 4952.
[5] J. Y. Wong, R. Langer, D. E. Ingber, *Proc. Natl. Acad. Sci. USA* **1994**, *91*, 3201.
[6] S. Inal, A. Hama, M. Ferro, C. Pitsalidis, J. Oziat, D. Iandolo, A.-M. Pappa, M. Hadida, M. Huerta, D. Marchat, P. Mailley, R. M. Owens, *Adv. Biosyst.* **2017**, *1*, 1700052.
[7] I. del Agua, S. Marina, C. Pitsalidis, D. Mantione, M. Ferro, D. Iandolo, A. Sanchez-Sanchez, G. G. Malliaras, R. M. Owens, D. Mecerreyes, *ACS Omega* **2018**, *3*, 7424.
[8] A. K. Jayaram, C. Pitsalidis, E. Tan, C. M. Moysidou, M. F. L. De Volder, J. S. Kim, R. M. Owens, *Front. Chem.* **2019**, *7*, 363.
[9] B. Zhu, S. C. Luo, H. Zhao, H. A. Lin, J. Sekine, A. Nakao, C. Chen, Y. Yamashita, H. H. Yu, *Nat. Commun.* **2014**, *5*, 4523.
[10] A. Dominguez-Alfaro, N. Alegret, B. Arnaiz, M. Salsamendi, D. Mecerreyes, M. Prato, *ACS Appl. Mater. Interfaces* **2020**, *12*, 57330.
[11] S. Song, D. Amores, C. Chen, K. McConnell, B. Oh, A. Poon, P. M. George, *Sci. Rep.* **2019**, *9*, 19565.
[12] A. Magaz, B. F. Spencer, J. G. Hardy, X. Li, J. E. Gough, J. J. Blaker, *ACS Biomater. Sci. Eng.* **2020**, *6*, 6906.
[13] C. D. McCaig, B. Song, A. M. Rajnicek, *J. Cell Sci.* **2009**, *122*, 4267.
[14] C. E. Schmidt, V. R. Shastri, J. P. Vacanti, R. Langer, *Proc. Natl. Acad. Sci. U.S.A.* **1997**, *94*, 8948.
[15] S. Sirivisoot, R. Pareta, B. S. Harrison, *Interface Focus* **2014**, *4*, 20130050.
[16] Z. Wang, Z. Wang, W. W. Lu, W. Zhen, D. Yang, S. Peng, *NPG Asia Mater.* **2017**, *9*, e435.
[17] N. Alegret, A. Dominguez-Alfaro, D. Mecerreyes, *Biomacromolecules* **2019**, *20*, 73.
[18] S. Vijayavenkataraman, S. Kannan, T. Cao, J. Y. H. Fuh, G. Sriram, W. F. Lu, *Front. Bioeng. Biotechnol.* **2019**, *7*, 266.
[19] S. Baek, R. A. Green, L. A. Poole-Warren, *Acta Biomater.* **2014**, *10*, 3048.
[20] J. Rivnay, S. Inal, B. A. Collins, M. Sessolo, E. Stavrinidou, X. Strakosas, C. Tassone, D. M. Delongchamp, G. G. Malliaras, *Nat. Commun.* **2016**, *7*, 11287.
[21] G. B. Tseghai, D. A. Mengistie, B. Malengier, K. A. Fante, L. Van Langenhove, *Sensors (Basel)* **2020**, *20*, 1881.
[22] S. Venkatraman, J. Hendricks, Z. A. King, A. J. Sereno, S. Richardson-Burns, D. Martin, J. M. Carmena, *IEEE Trans. Neural Syst. Rehabil. Eng.* **2011**, *19*, 307.
[23] C. Pitsalidis, A. M. Pappa, A. J. Boys, Y. Fu, C. M. Moysidou, D. Van Niekerk, J. Saez, A. Savva, D. Iandolo, R. M. Owens, *Chem. Rev.* **2022**, *122*, 4700.
[24] M. Garcia-Hernando, J. Saez, A. Savva, L. Basabe-Desmonts, R. M. Owens, F. Benito-Lopez, *Biosens. Bioelectron.* **2021**, *191*, 113405.
[25] D. Iandolo, J. Sheard, G. Karavitas Levy, C. Pitsalidis, E. Tan, A. Dennis, J. S. Kim, A. E. Markaki, D. Widera, R. M. Owens, *MRS Commun.* **2020**, *10*, 179.
[26] R. Zierold, J. Harberts, C. Fendler, J. Teuber, M. Siegmund, A. Silva, N. Rieck, M. Wolpert, R. H. Blick, *ACS Nano* **2020**, *14*, 13091.
[27] R. Lozano, L. Stevens, B. C. Thompson, K. J. Gilmore, R. Gorkin, E. M. Stewart, M. in het Panhuis, M. Romero-Ortega, G. G. Wallace, *Biomaterials* **2015**, *67*, 264.
[28] A. Odawara, M. Gotoh, I. Suzuki, *RSC Adv.* **2013**, *3*, 23620.
[29] X. Li, S. Liu, Y. Zhao, J. Li, W. Ding, S. Han, B. Chen, Z. Xiao, J. Dai, *Adv. Funct. Mater.* **2016**, *26*, 5835.
[30] C. D. Spicer, A. Gelmi, J. F. Ponder Jr, R. Vilar, A. Serio, K. I. Ritzau-Reid, C. D. Spicer, A. Gelmi, C. L. Grigsby, J. F. Ponder Jr, V. Bemmer,

A. Creamer, R. Vilar, A. Serio, M. M. Stevens, K. I. Ritzau-Reid, A. V. Gelmi Bemmer, A. Creamer, M. M. Stevens, C. L. Grigsby, *Adv. Funct. Mater.* **2020**, *30*, 2003710.
[31] S. Bosi, R. Rauti, J. Laishram, A. Turco, D. Lonardoni, T. Nieus, M. Prato, D. Scaini, L. Ballerini, *Sci. Rep.* **2015**, *5*, 9562.
[32] R. Boni, A. Ali, A. Shavandi, A. N. Clarkson, *J. Biomed. Sci.* **2018**, *25*, 90.
[33] S. Ullah, X. Chen, *Appl. Mater. Today* **2020**, *20*, 100656.
[34] S. Afewerki, A. Sheikhi, S. Kannan, S. Ahadian, A. Khademhosseini, *Bioeng. Transl. Med.* **2019**, *4*, 96.
[35] C. M. Moysidou, C. Barberio, R. M. Owens, *Front. Bioeng. Biotechnol.* **2021**, *8*, 620962.
[36] J. Gansau, C. T. Buckley, *J. Funct. Biomater.* **2018**, *9*, 43.
[37] M. Talovic, M. Marcinczyk, N. Ziemkiewicz, K. Garg, *Adv. Tissue Eng. Regen. Med. Open Access* **2017**, *2*, 194.
[38] X. Liu, C. Zheng, X. Luo, X. Wang, H. Jiang, *Mater. Sci. Eng., C* **2019**, *99*, 1509.
[39] J. D. Malcor, E. J. Hunter, N. Davidenko, D. V. Bax, R. Cameron, S. Best, S. Sinha, R. W. Farndale, *Regener. Biomater.* **2021**, *7*, 471.
[40] A. Martínez, M. D. Blanco, N. Davidenko, R. E. Cameron, *Carbohydr. Polym.* **2015**, *132*, 606.
[41] N. Alegret, A. Dominguez-Alfaro, J. M. González-Domínguez, B. Arnaiz, U. Cossío, S. Bosi, E. Vázquez, P. Ramos-Cabrer, D. Mecerreyes, M. Prato, *ACS Appl. Mater. Interfaces* **2018**, *10*, 43904.
[42] S. M. Richardson-Burns, J. L. Hendricks, D. C. Martin, *J. Neural Eng.* **2007**, *4*, L6.
[43] N. Sultana, H. C. Chang, S. Jefferson, D. E. Daniels, *J. Pharm. Invest.* **2020**, *50*, 437.
[44] R. Rauti, N. Renous, B. M. Maoz, *Isr. J. Chem.* **2020**, *60*, 1141.
[45] D. Lam, H. A. Enright, J. Cadena, S. K. G. Peters, A. P. Sales, J. J. Osburn, D. A. Soscia, K. S. Kulp, E. K. Wheeler, N. O. Fischer, *Sci. Rep.* **2019**, *9*, 4159.
[46] S. R. Moxon, N. J. Corbett, K. Fisher, G. Potjewyd, M. Domingos, N. M. Hooper, *Mater. Sci. Eng., C* **2019**, *104*, 109904.
[47] M. P. Ferro, S. C. Heilshorn, R. M. Owens, *Mater. Sci. Eng., R* **2020**, *140*, 100522.
[48] C. Wang, S. S. Rubakhin, M. J. Enright, J. V. Sweedler, R. G. Nuzzo, *Adv. Funct. Mater.* **2021**, *31*, 2010246.
[49] A. J. Bastiaens, J. P. Frimat, T. van Nunen, B. Schurink, E. F. G. A. Homburg, R. Luttge, *Front. Mech. Eng.* **2018**, *4*, 21.
[50] M. G. Evans, A. Al-Shakli, D. M. Chari, *Integr. Biol. (Camb)*. **2019**, *11*, 395.
[51] N. Schaefer, D. Janzen, E. Bakirci, A. Hrynevich, P. D. Dalton, C. Villmann, *Adv. Healthcare Mater.* **2019**, *8*, 1801226.
[52] J. Zeng, N. Sasaki, C. R. Correia, J. F. Mano, M. Matsusaki, *Small* **2020**, *16*, 1907434.
[53] T. M. Kruger, K. J. Bell, T. I. Lansakara, A. V. Tivanski, J. A. Doorn, L. L. Stevens, *ACS Chem. Neurosci.* **2020**, *11*, 840.
[54] J. Z. Yeh, D. H. Wang, J. H. Cherng, Y. W. Wang, G. Y. Fan, N. H. Liou, J. C. Liu, C. H. Chou, *Polymers* **2020**, *12*, 2245.
[55] W. Lee, J. Pinckney, V. Lee, J.-H. Lee, K. Fischer, S. Polio, J.-K. Park, S.-S. Yoo, *Neuroreport* **2009**, *20*, 798.
[56] H. Kenar, C. Y. Ozdogan, C. Dumlu, E. Doger, G. T. Kose, V. Hasirci, *Mater. Sci. Eng., C* **2019**, *97*, 31.
[57] S. Grabska-Zielińska, A. Sionkowska, K. Reczyńska, E. Pamuła, *Polymers (Basel)* **2020**, *12*, 372.
[58] Y. He, Z. Hou, J. Wang, Z. Wang, X. Li, J. Liu, X. Yang, Q. Liang, J. Zhao, *Int. J. Biol. Macromol.* **2020**, *149*, 1275.
[59] L. Kang, W. Jia, M. Li, Q. Wang, C. Wang, Y. Liu, X. Wang, L. Jin, J. Jiang, G. Gu, Z. Chen, *Carbohydr. Polym.* **2019**, *223*, 115106.
[60] D. B. Unal, S. R. Caliari, K. J. Lampe, *Brain Res. Bull.* **2019**, *152*, 159.
[61] S. A. Kruse, G. H. Rose, K. J. Glaser, A. Manduca, J. P. Felmlee, C. R. Jack, R. L. Ehman, *Neuroimage* **2008**, *39*, 231.
[62] S. W. Moore, M. P. Sheetz, *Dev. Neurobiol.* **2011**, *71*, 1090.
[63] E. Axpe, G. Orive, K. Franze, E. A. Appel, *Nat. Commun.* **2020**, *11*, 3423.
[64] S. Wang, S. Guan, J. Xu, W. Li, D. Ge, C. Sun, T. Liu, X. Ma, *Biomater. Sci.* **2017**, *5*, 2024.
[65] M. J. Donahue, A. Sanchez-Sanchez, S. Inal, J. Qu, R. M. Owens, D. Mecerreyes, G. G. Malliaras, D. C. Martin, *Mater. Sci. Eng., R* **2020**, *140*, 100546.
[66] S. Wang, S. Guan, Z. Zhu, W. Li, T. Liu, X. Ma, *Mater. Sci. Eng., C* **2017**, *71*, 308.
[67] J. Kucinska-Lipka, M. Marzec, I. Gubanska, H. Janik, *J. Elastomers Plast.* **2017**, *49*, 440.
[68] C. M. Moysidou, R. M. Owens, C. Pitsalidis, M. Al-Sharabi, A. Withers, J. A. Zeitler, *Adv. Biol.* **2021**, *5*, 2000306.
[69] J. Kovalevich, D. Langford, *Methods Mol. Biol.* **2013**, *1078*, 9.
[70] M. M. Shipley, C. A. Mangold, M. L. Szpara, *J. Visualized Exp.* **2016**, *108*, 53193.
[71] I. Vetter, C. A. Mozar, T. Durek, J. S. Wingerd, P. F. Alewood, M. J. Christie, R. J. Lewis, *Biochem. Pharmacol.* **2012**, *83*, 1562.
[72] J. I. Forster, S. Köglsberger, C. Trefois, O. Boyd, A. S. Baumuratov, L. Buck, R. Balling, P. M. A. Antony, *J. Biomol. Screening* **2016**, *21*, 496.
[73] J. R. Murillo, L. Goto-Silva, A. Sánchez, F. C. S. Nogueira, G. B. Domont, M. Junqueira, *EuPA Open Proteomics* **2017**, *16*, 1.
[74] S. B. Yoon, G. Lee, S. B. Park, H. Cho, J. O. Lee, B. Koh, *RSC Adv.* **2020**, *10*, 19382.
[75] M. Şahin, G. Öncü, M. A. Yılmaz, D. Özkan, H. Saybaşılı, *Neurosci. Lett.* **2021**, 745, 135628.
[76] C. Pitsalidis, M. P. Ferro, D. Iandolo, L. Tzounis, S. Inal, R. M. Owens, *Sci. Adv.* **2018**, *4*, eaat4253.
[77] J. Gordon, S. Amini, M. K. White, *Methods Mol. Biol.* **2013**, *1078*, 1.
[78] M. Innala, I. Riebe, V. Kuzmenko, J. Sundberg, P. Gatenholm, E. Hanse, S. Johannesson, *Artif. Cells Nanomed. Biotechnol.* **2014**, *42*, 302.
[79] M. Bordoni, E. Karabulut, V. Kuzmenko, V. Fantini, O. Pansarasa, C. Cereda, P. Gatenholm, *Cells* **2020**, *9*, 682.
[80] J. Johnston, I. D. Forsythe, C. Kopp-Scheinpflug, *J. Physiol.* **2010**, *588*, 3187.
[81] F. Tamagnini, D. A. Walsh, J. T. Brown, M. K. Bondulich, D. P. Hanger, A. D. Randall, *Neurobiol. Aging* **2017**, *60*, 44.
[82] D. Prè, M. W. Nestor, A. A. Sproul, S. Jacob, P. Koppensteiner, V. Chinchalongporn, M. Zimmer, A. Yamamoto, S. A. Noggle, O. Arancio, *PLoS One* **2014**, *9*, e103418.
[83] K. Chwalek, M. D. Tang-Schomer, F. G. Omenetto, D. L. Kaplan, *Nat. Protoc.* **2015**, *10*, 1362.
[84] V. F. Curto, B. Marchiori, A. Hama, A. M. Pappa, M. P. Ferro, M. Braendlein, J. Rivnay, M. Fiocchi, G. G. Malliaras, M. Ramuz, R. M. Owens, *Microsyst. Nanoeng.* **2017**, *3*, 17028.
[85] C. Pitsalidis, M. P. Ferro, D. Iandolo, L. Tzounis, S. Inal, R. M. Owens, *Sci. Adv.* **2018**, *4*, 10.
[86] C. M. Moysidou, R. M. Owens, *Biochem. Soc. Trans.* **2021**, *49*, 187.
[87] S. Santillo, A. S. Moriello, V. Di Maio, *Gen. Physiol. Biophys.* **2014**, *33*, 121.